POLITECNICO DI TORINO
Repository ISTITUZIONALE

Effective strategy for UV-mediated grafting of biocidal Ag-MOFs on polymeric membranes aimed at enhanced water ultrafiltration

(Article begins on next page)

22 May 2025

Effective strategy for UV-mediated grafting of biocidal Ag-MOFs on polymeric membranes aimed at enhanced water ultrafiltration

Mehdi Pejman,[a,1] Mostafa Dadashi Firouzjaei,[b,1] Sadegh Aghapour Aktij,[c,d] Ehsan Zolghadr,[b,e] Parnab Das,[b] Mark Elliott,[b,*] Mohtada Sadrzadeh,[c] Marco Sangermano,[f] Ahmad Rahimpour,[a,f,g*] and Alberto Tiraferri[a,*]

[a] Department of Environment, Land and Infrastructure Engineering (DIATI), Politecnico di Torino, Corso Duca degli Abruzzi 24, 10129 Turin, Italy

[b] Department of Civil, Construction, and Environmental Engineering, University of Alabama, Tuscaloosa 35487, USA

[c] Department of Mechanical Engineering, 10-367 Donadeo Innovation Center for Engineering, Advanced Water Research Lab (AWRL), University of Alberta, Edmonton, AB, T6G 1H9, Canada

[d] Department of Chemical & Materials Engineering, University of Alberta, Edmonton, AB T6G 1H9, Canada

[e] Department of Physics and Astronomy, University of Alabama, Tuscaloosa, AL, 35487, USA

[f] Department of Applied Science and Technology, Politecnico di Torino, Corso Duca Degli Abruzzi 24, 10129, Turin, Italy

[g] Chemical Engineering Department, Babol Noshirvani University of Technology, Shariati Ave., Babol 4714781167, Iran

[1]These authors contributed equally to this work
*Corresponding Authors

Highlights

- Acrylic acid and Ag-MOFs are UV-grafted on UF membranes via a photo initiator.

- UV-grafted membranes show improved water wettability and antifouling function.

- Reduced flux decline with consistently high rejection observed for modified membranes.

- In-situ formation of Ag-MOFs on pre-grafted acrylic acid provides the best surface properties.

- MOF-modified membranes have excellent biocidal activity against *E. coli* and *S. aureus*.

ABSTRACT

Ultrafiltration membranes with antifouling and antibacterial properties are greatly beneficial for all industrial applications and to supply safe water worldwide. Improving these properties while maintaining both high productivity and high product water quality remains a challenge. This work proposes the surface functionalization of an ultrafiltration membrane obtained via UV-initiated grafting polymerization of acrylic acid (AA) and silver-containing metal-organic frameworks (Ag-MOFs), with the goal to achieve combined bactericidal and hydrophilic properties. The effectiveness of different modification pathways is evaluated, including Ag-MOFs blending into the AA solution followed by grafting, as well as in-situ synthesis of Ag-MOFs over the surface of AA-grafted membranes, with in-depth characterization of the resulting materials. The steady-state water fluxes with a feed water laden with organics are improved from two to three-fold for the functionalized membranes compared to the commercial one, while the rejection of macromolecules is maintained at >99%. Significantly, fouling is partly reversible with all enhanced surfaces: the flux recovery ratio following cleaning varies between 3.8% and 20% compared to near zero for the pristine membrane. Noteworthy bacterial inactivation reaches up to 90% for *E. coli* and 95% for *S. aureus*, respectively, for surface-grafted membranes. Silver leaching and surface characterization analyses indicate a strong immobilization of Ag-MOFs on membranes and imply long-lasting antimicrobial as well as antifouling activities.

*In-Situ Fabrication of Ag-MOF on Polysulfone Membrane
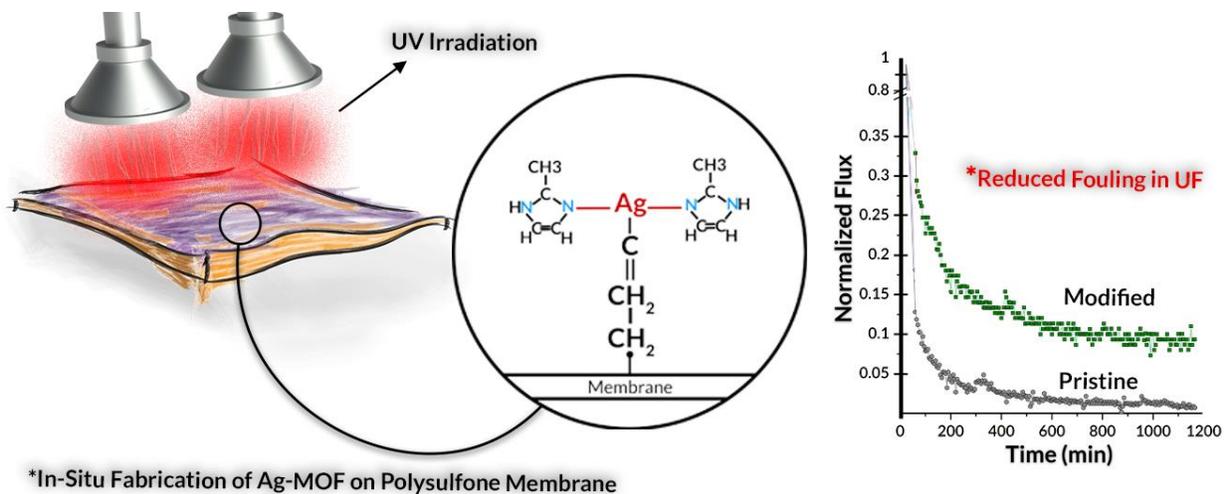
Keywords: Ultrafiltration; UV irradiation; Metal organic frameworks; antifouling; antibacterial activity.

1. Introduction

The supply of freshwater is constantly being intensified given the growing population and climate change adaptation measures, putting stress on our conventional surface water and groundwater resources [1]. At the same, industrial activities are increasing as well as changing the variety and the nature of (micro)pollutants introduced into our water sources through wastewater, thus calling for constant innovation in technologies to better purify these streams [2]. Ultrafiltration (UF) membranes are widely used for the treatment and pre-treatment of contaminated waters [3, 4]. The pore size of UF membranes denies passage to a wide spectrum of pollutants, including medium to high molecular weight compounds, suspended particles, bacteria, and viruses [3]. The majority of UF membranes are synthesized from polymers: polymeric UF membranes, despite their widespread application, do face some critical drawbacks, the most detrimental of which is fouling [5, 6].

Fouling occurs when retained microorganisms, colloidal particles, organic matter, and scaling agents deposit either at the membrane surface or within its pores [7]. Major fouling mechanisms include adsorption, chemical interaction, cake layer formation, and pore blocking [8], the rates of which depend on factors such as foulant concentration and surface pore distribution [9]. The resulting deposited layer or pore blockage is detrimental to permeate flux and/or membrane selectivity, with energy costs increasing due to a need for higher applied pressures [10]. Fouling potential correlates well to membrane material and more specifically, with its surface morphology and chemistry. Indeed, tailoring the membrane surface could be highly effective in improving its performance and sustaining surface integrity over prolonged operations. Understanding and designing the solid-liquid membrane/water interface could lead not only to reduced fouling, but also lower energy requirements for the treatment process [11].

Within surface modification strategies for UF membranes, using materials that contain amine and carboxyl groups has proven advantageous in combating fouling by increasing the wettability of otherwise relatively hydrophobic polymeric membranes [12]. Also, introducing an antibacterial agent onto the membrane surface can add an additional disinfection function to the membrane, making it a dual-barrier separation system, also resistant towards biofilm formation [13]. Specifically, it has been shown that anchoring silver-containing nanoparticles arms the membrane with antimicrobial properties via both direct contact killing and silver release: these mechanisms can enhance the membrane resilience against the deposition and activity of viruses, bacteria, and fungi [14, 15]. However, there are challenges facing this approach, including loose silver immobilization, which results in loss of materials and function during membrane operation and cleaning [16, 17], as well as inherent incompatibility between the inorganic nature of silver and the organic matrix of the polymer, which results in defect formation and compromised selectivity [18].

Metal-organic-frameworks (MOFs) are a group of coordination polymers comprising metal nodes linked by organic ligands [19, 20]. These networks benefit from tunability through the choice of both metal and ligand, thus allowing greater compatibility with the polymer matrix compared to fully inorganic structures [21, 22]. Also, in these structures, the organic frame can act as a barrier against high rates of metal loss [8, 21]. MOFs prevent the aggregation of nanoparticles and provide uniform distribution of biocidal agents across the membrane surface [23]. There are various ways of adding MOFs to the polymeric surface of membranes, such as surface grafting [24, 25], layer by layer assembly [26, 27], in-situ surface functionalization, and direct deposition of MOFs [28, 29]. As the separation properties of the separation medium are

defined by the uppermost few nanometers of its thickness, implementing modifications in the manner of post-fabrication surface functionalization is an attractive approach [28, 29].

One efficient yet facile method of irreversible surface functionalization is realized under UV-irradiation. Surface functionalization can be achieved either through the "grafting to" or "grafting from" technique. In "grafting to", end-functionalized polymer molecules react with functional groups on the surface in order to form tethered chains [30]. On the other hand, the "grafting from" technique starts at the substrate level by (normally covalently) attached initiating groups. Consequently, the second monomer molecules can easily permeate into and across the already established grafted layer, allowing for advantages in terms of uniformity and density of surface deposition [30, 31]. One of the most popular "grafting from" pathways, initially introduced by Ma et al. [32] to modify polypropylene membranes, is through a 2-step process to form a secondary layer of UV-grafted polymeric surface, mediated by benzophenone (BP) as a photo initiator [32]. Wu *et al.* [33] provided a comprehensive review on molecular engineering in organic-inorganic interfaces to obtain functional separation membranes that can also guide membrane surface functionalization.

In this work, we functionalize the surface of polymeric UF membranes with silver-containing antibacterial MOFs (Ag-MOFs) through BP-assisted UV photo-grafting of acrylic acid (AA). First, BP was used as an initiator for UV-grafting of AA onto the membrane, thus preparing the surface for in-situ MOFs synthesis and growth. In fact, the grafted hydrophilic AA layer itself combats fouling while also providing a reactive site for further additives [12, 34-36]. These AA-seeded membranes are thus functionalized with Ag-MOFs to impart additional antibacterial activity. Using Ag-MOFs (as opposed to conventional silver nanoparticles) could lead to more polymer compatibility with the membrane, silver stability through proper

scaffolding [37] and thus, less toxicity through controlled silver release [28, 38, 39]. Also, accommodating a hydrophilic base layer via the "grafting from" pathway leads to a potential increase in Ag binding sites and more efficient antifouling [28, 29]. To our knowledge, this is the first work to exploit the capacity of AA UV photo-grafting to introduce the Ag-MOFs biocidal agents to a membrane. Subsequent to functionalization, membranes are characterized to verify the presence of newly grafted molecules and investigate the obtained physio-chemical properties. These membranes are tested in a UF filtration setup to evaluate their performance in terms of flux, humic acid retention, and fouling behavior. Their antibacterial propensity is discussed on the basis of both disc inhibition zone and confocal microscopy tests. Finally, the rate of silver release is also evaluated to preliminarily assess the environmental sustainability and log-term function of the fabricated membranes.

2. Experimental

2.1 Reagents

Silver nitrate ($AgNO_3$, Sigma-Aldrich) and 2-methylimidazole (2MI, Sigma-Aldrich) were used as sources of metal and ligand, respectively, for the preparation of Ag-MOFs. Water and ethanol (Acros Organics) were used as solvents to prepare the metal and ligand solutions, respectively. Benzophenone (BP, Sigma-Aldrich) was used as a photo-initiating agent, in a UV chamber (Dymax ECE 5000) that employs an irradiation wavelength within the UV-A range (365 nm wavelength) and utilized to house the membrane samples for surface functionalization. Acrylic acid (AA, Acros Organics) was used as a hydrophilic monomer for membrane surface grafting. Commercial M-PS20-GPET ultrafiltration membranes purchased from Nanostone Water were immersed in aqueous solution at pH 11 overnight to wash off any coating agent

before functionalization or direct use as pristine materials. Deionized water (DI) was used for all purposes.

2.2 Surface modification of UF membranes

Different membrane functionalization strategies were compared for the purposes of this study, for a total of five sets of samples, including the pristine polysulfone (PSf) membrane, denoted as U0. The hydrophilic AA monomers were grafted onto U0 via dip-coating followed by UV irradiation, to obtain membranes referred to as U1. This procedure was carried out in two steps: in the first step, the membranes were immersed in a methanol solution containing 0.3 wt.% of BP for 30 min. BP-soaked membranes were then subjected to irradiation in the UV chamber for 5 min. In the second step, the BP-activated membrane samples were immersed in 5 wt.% of AA solution for 30 min. The AA-soaked membranes were then again UV irradiated for 5 min.

Two sets of membranes, U2 and U3, were functionalized with both AA and Ag-MOFs, following two separate modification pathways. The first step of modification, i.e., UV-mediated BP grafting, was achieved similarly to U1, while the introduction of AA and Ag-MOFs was performed in the second step of modification. In the first pathway, 0.1 wt.% of Ag-MOFs powder (synthesized according to our previously published paper [29]) was dispersed in AA solution and poured on top of the membranes before a second UV irradiation (U2). In the second pathway, Ag-MOFs were in-situ synthesized over the surface of U1 membranes (to obtain U3). Specifically, AA photo-grafted membranes were soaked with $AgNO_3$ solution (0.6 gr in 90 mL DI) for 30 min followed by 30 min of soaking with 2MI solution (1.05 gr in 90 mL ethanol). Negative carboxyl functional groups of AA photo-grafted surfaces can act as active sites to boost the nucleation of Ag^+ ions on the membrane surface [40, 41]. All UV-irradiated samples were subsequently rinsed several times with methanol and dried at 50 °C for 1 h. To better evaluate

9

the modification procedure described above, Ag-MOFs were also in-situ grown over the surface of pristine PSf U0 membranes, without any intermediate functionalization; these samples are referred to as U4. The step-by-step functionalization procedures are illustrated in Figure 1.
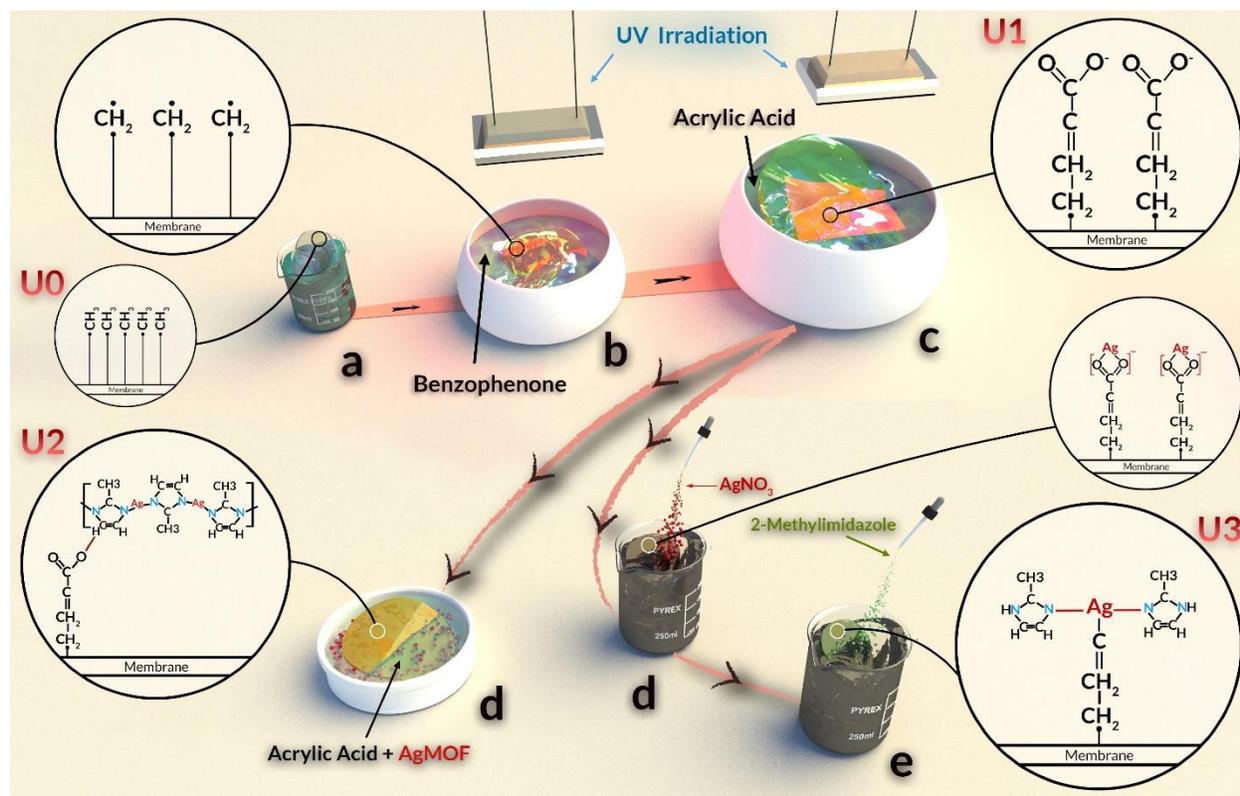
Figure 1. Illustration of membrane modification steps to obtain different membrane surface modifications. U0: pristine PSf membrane; U1: AA photo-grafted membrane; U2: Ag-MOFs-coated AA photo-grafted membrane; U3: in-situ synthesized Ag-MOFs on the surface of AA photo-grafted membrane; U4 (not shown in the figure): in-situ synthesized Ag-MOFs on the surface of pristine PSf membrane.

2.3 Characterization of the materials

The membranes were characterized using a variety of techniques and devices. The surface functionalities were evaluated with attenuated total reflection Fourier transform infrared spectroscopy (ATR-FTIR, Nicolet iS50 FT, Thermo Fisher Scientific, USA), set between 500

and 4000 cm^{-1}. Surface morphology was observed using scanning electron microscopy (SEM, JEOL 7000, JEOL, USA) equipped with energy-dispersive X-ray spectroscopy (EDX, JEOL 7000, JEOL, USA). A 5-nm gold layer was coated on the membranes using a sputter coater (Leica EM ACE600, USA) before measurements. Further investigation of surface topology and roughness analysis was provided via atomic force microscopy (AFM, Bruker Dimension Edge, USA). The AFM probe tip cannot access pores and the tip/surface interaction convolution may be prone to artifacts; however, this technique allows estimation of obvious changes of roughness in the order of tens of nanometers for evaluation of the effects of surface modification on R_a (average roughness) and R_{RMS} (root-mean-squared roughness), relevant for filtration performance. Membrane wettability was evaluated using contact angle measurements (DSA 100, KRÜSS, Germany) of water droplets on five different spots for each sample. Functional groups and elements present on the surface of the membranes were identified using X-ray photoelectron spectroscopy (XPS) performed with a Kratos spectrometer (Axis 165 XPS/ Auger, Shimadzu, Japan) equipped with a 100 μm monochromatic Al K(alpha) X-ray.

2.4 Filtration experiments and evaluation of fouling behavior

Membrane coupons with an effective area of 3.8 cm^2 were used in a dead-end cell (model 8010, Amicon). The pressure was applied with a pressurized nitrogen gas tank and all filtration steps were carried out with the cells being stirred at 200 rpm. The membranes were initially compacted using DI as feed solution under 4 bar applied pressure (for 2 h to reach a steady flux). Subsequently, DI water permeation flux was measured and recorded at 2 bar for 1 h (J_{w1}). A 200 ppm humic acid (HA) solution containing 10 mM NaCl, 0.1 mM NaHCO$_3$ (pH 7), and 0.5 mM CaCl$_2$ was used as model foulant solution to evaluate HA filtration flux (J_p), rejection, and fouling behavior, starting with an initial flux of 600 ± 100 L m^{-2}h^{-1} (roughly 3 bar applied

pressure for all membranes). The water permeability coefficient, PWP (L m^{-2} h^{-1}bar^{-1}), and the rejection rate of HA were determined using equations (1) and (2):

$$PWP = \frac{J_{w1}}{\Delta p} \qquad (1)$$

$$R\% = \left(1 - \frac{Cp}{Cf}\right) \times 100 \qquad (2)$$

where Δp is the transmembrane pressure, $R\%$ is the rejection rate, and C_p and C_f are the solute concentrations in the permeate and feed solution, respectively. Upon completion of the filtration period, the membranes were physically washed with DI water for 10 min and tested again to investigate the flux recovery for 1 h (J_{w2}) using DI water as feed solution and under a 2 bar pressure. The flux recovery ratio (FRR%) were measured based on the following formula:

$$FRR\% = \left(\frac{J_{w2}}{J_{w1}}\right) \times 100 \qquad (3)$$

All fluxes during the fouling run are reported in the normalized format (relative to the starting flux) for easier comparative analysis of the fouling behaviour. Fouling was further categorized as total fouling ratio ($R_{t\%}$), reversible fouling ratio ($R_{r\%}$), and irreversible fouling ratio ($R_{ir\%}$) according to equations below [26, 42]:

$$(\%) = \left(1 - \frac{Jp}{Jw1}\right) \times 100 \qquad (4)$$

$$Rir(\%) = \left(1 - \frac{Jw2}{Jw1}\right) \times 100 \qquad (5)$$

$$Rr(\%) = \left(\frac{Jw2 - Jp}{Jw1}\right) \times 100 \qquad (6)$$

2.5. Evaluation of antibacterial activity

The assessment of antibacterial properties of the membranes was carried out using the methodology described in detail in our previous studies [29, 43]. Briefly, *Escherichia coli* (*E. coli*) and *Staphylococcus aureus* (*S. aureus*) were chosen as gram-negative and gram-positive

model bacteria, respectively. For confocal microscopy experiments, the viability of bacterial cells on the membranes was determined with a LIVE/DEAD BacLight bacterial viability kit. Both *E. coli* and *S. aureus* were grown overnight, and the suspensions were placed in contact with the membrane surfaces. Afterwards, the samples were stained with propidium iodide (PI) (that can only cross compromised bacterial membranes) and then SYTO 9 (universal stain that crosses intact cell membranes) and incubated for 15 min. A Nikon C2 laser scanning confocal microscope was then used to take images of the membrane surface, which were analyzed with ImageJ to count the proportion of attached bacteria stained with PI (red color, non-viable cells) or with SYTO 9 (green color, viable cells). For disc inhibition tests, a bacterial suspension with 10^6 CFU/mL of *E. coli* or *S. aureus* was spread on a petri dish containing trypticase soy agar. Membrane discs with a diameter of 12 mm were then placed facing downward in the middle of the petri dish and incubated for 18 h. A Canon 1200d camera was used to take pictures of the inhibited area on the membranes.

3. Results and discussion

### 3.1. Physio-chemical and morphological properties of the modified surfaces

3.1.1 Surface composition

The successful grafting of AA on U1, U2, and U3 membranes and, specifically, the presence of carboxyl groups necessary for further functionalization of the surface with Ag-MOFs, was investigated by ATR-FTIR spectroscopy, with results reported in Figure 2a. Peaks at 1150 cm^{-1}, 1242 cm^{-1}, 1489 cm^{-1}, and 1585 cm^{-1} are characteristic peaks of PSf, respectively, due to the symmetric stretching vibrations of O=S=O [43], O-C-O asymmetric stretching [43, 44], and the aromatic ring stretching of both functionalities [44, 45]. Furthermore, the detected peak at around 1324 cm^{-1} is reportedly caused by the asymmetric vibrations of O=S=O [46].

Additionally, multiple peaks in the range of 834-692 cm^{-1} likely associated with the rocking and bending vibrations of C–H [46, 47]. Notably, an extra peak at 1725 cm^{-1} appeared only in the FTIR spectra of U1, U2, and U3. This peak is the characteristic peak for the carbonyl group (C=O stretching) [36, 47]. This outcome suggests the successful modification of membranes, as the C=O bond comes from the acrylic acid and does not pre-exist in the PSf structure. Accordingly, this signal was not detected in the spectra of U0 and U4, for which acrylic acid was not present.

To verify the occurrence of Ag-MOFs in U2, U3, and U4 and semi-quantitatively determine the extent of their presence, XPS spectra were obtained and summarized in Figure 2b. Expectedly, all membranes showed peaks for carbon (C) and oxygen (O). The appearance of two prominent silver signals at about 367.5 and 373.5 eV, assigned to Ag $3d_{5/2}$ and $3d_{3/2}$, respectively, and mostly due to Ag−N bonding [28, 48], indeed indicates the existence of Ag-MOF on U2, U3, and U4 surfaces. These Ag peaks were more intense for U2 and U3 than U4 (respectively, 22 and 42 times larger based on the area under the curve), implying a more successful Ag-MOF deposition or formation on these sets of samples. These results indicate that using acrylic acid (AA) as a basis for subsequent coating with Ag-MOFs is a promising way to maximize surface functionalization. It is noteworthy to highlight that U3 contained about two times more Ag on the surface compared to U2, suggesting that the in-situ seeding and growth of MOF on AA carboxyl sites is more effective for grafting and possibly for structural bonding with MOFs. As further evidence of the presence of MOFs, all the membranes except U0 and U1 showed the peak attributed to nitrogen (N 1s) at 400 eV [40, 49, 50], originating from the 2-methyimidazole ligands [41, 51].

To corroborate the results obtained by FTIR analysis, the high-resolution peak associated with carbon (C 1s) and its corresponding deconvolution are evaluated (Figure 2c). The peak centered at 284.6 eV is assigned to C−C, C=C, C−S, and C−H bonds [52, 53] (C−N may also contribute for U2, U3, and U4 [41]) and the peak around 286.2 eV is ascribed to C−O and C−O−C bonds [54]. All these bonds pre-exist in the structure of PSf and were accordingly observed in the spectra of all the membranes. Notably, the third peak in C 1s appeared only in the spectra of U1, U2, and U3, which was approximately at 288.5 eV and may be attributed to C=O and O−C=O bonds [54]. Consistent with the results shown in Figure 2a, the C=O bond is likely related to AA incorporation. Correspondingly, this peak did not appear in the spectra of U0 and U4.
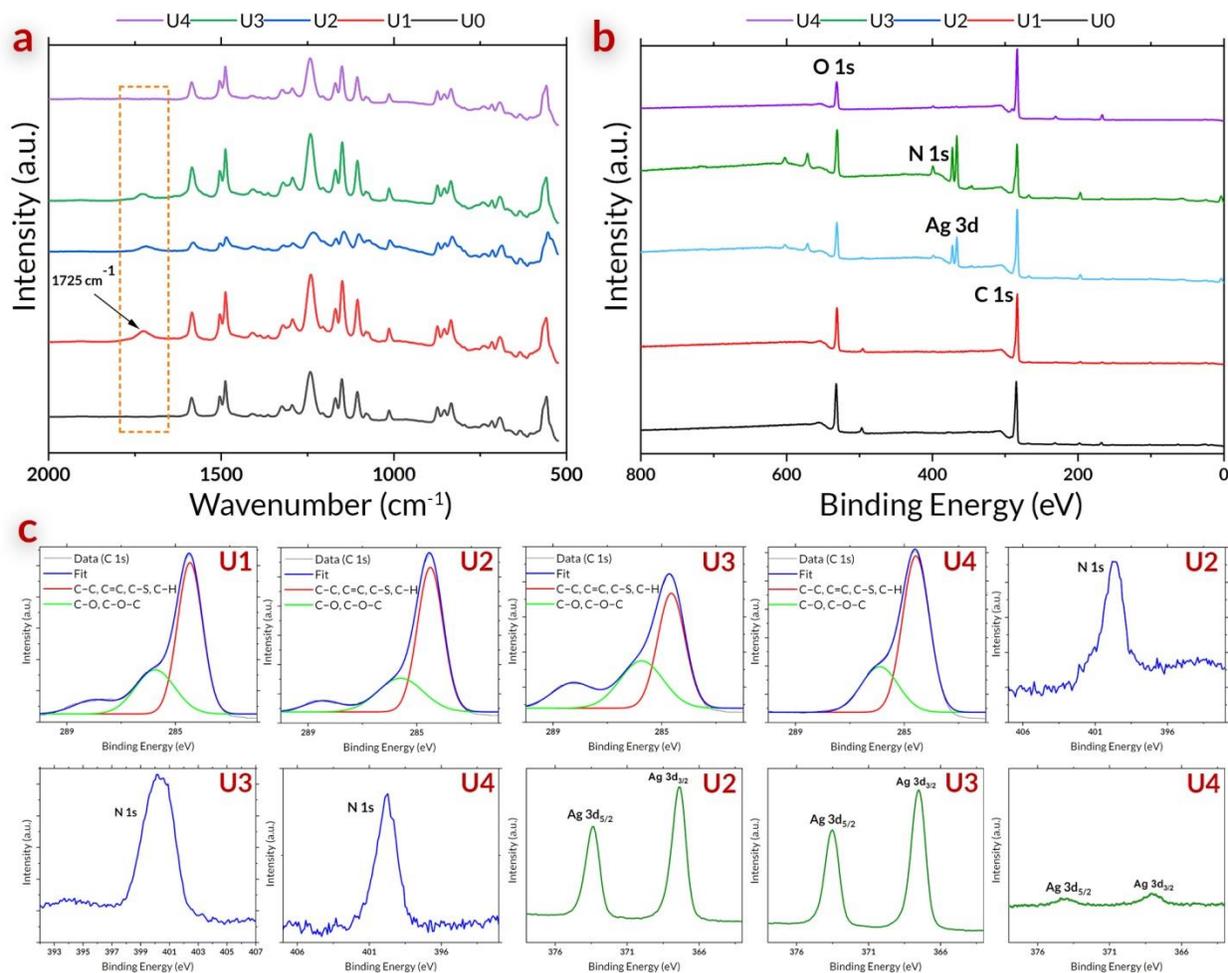
Figure 2. (a) ATR-FTIR spectra of the membranes; (b) XPS survey spectra and (c) high resolution deconvoluted XPS peaks of the membranes.

3.1.2 Surface morphology

Microscopy can provide indications of the morphology of the various membranes and the distribution of modifying agents. As evident in representative SEM micrographs (Figure 3a-e), several microscale and nanoscale aggregates were visible on the surface of U2, U3, and U4 samples, while not on U0 and U1 membranes. The black dots visible in the TEM images (Figure 3i, j, k) most probably correspond to Ag-MOFs. The presence of Ag-MOFs on U2 and U3 SEM

micrographs is observed to be different. U2 displayed a layer-like bed of smaller MOFs (~10-50 nm) because these MOFs were deposited from a suspension containing AA. On the other hand, the surface of U3 was covered with larger MOFs (~50-200 nm), which were in-situ grown on an already grafted AA layer. In both cases, the density and uniformity of MOF distribution were adequately high and potentially suitable to impart the desired surface properties to the membranes. Note that MOFs were also observed below the surface in U2 membranes, likely due to their penetration through the pores of the membrane during fabrication. In fact, the surface pore size of the commercial membranes was measured as 39 ± 15 nm, thus larger than a significant fraction of the MOF particles suspended in the AA solution for U2 modification. Instead, MOFs were only visible on the surface of U3 membranes, which is an ideal outcome given that the interaction with foulants and microorganisms occurs at this membrane/liquid interface, thus implying a more efficient use of chemicals and materials when in-situ growth approaches are adopted.
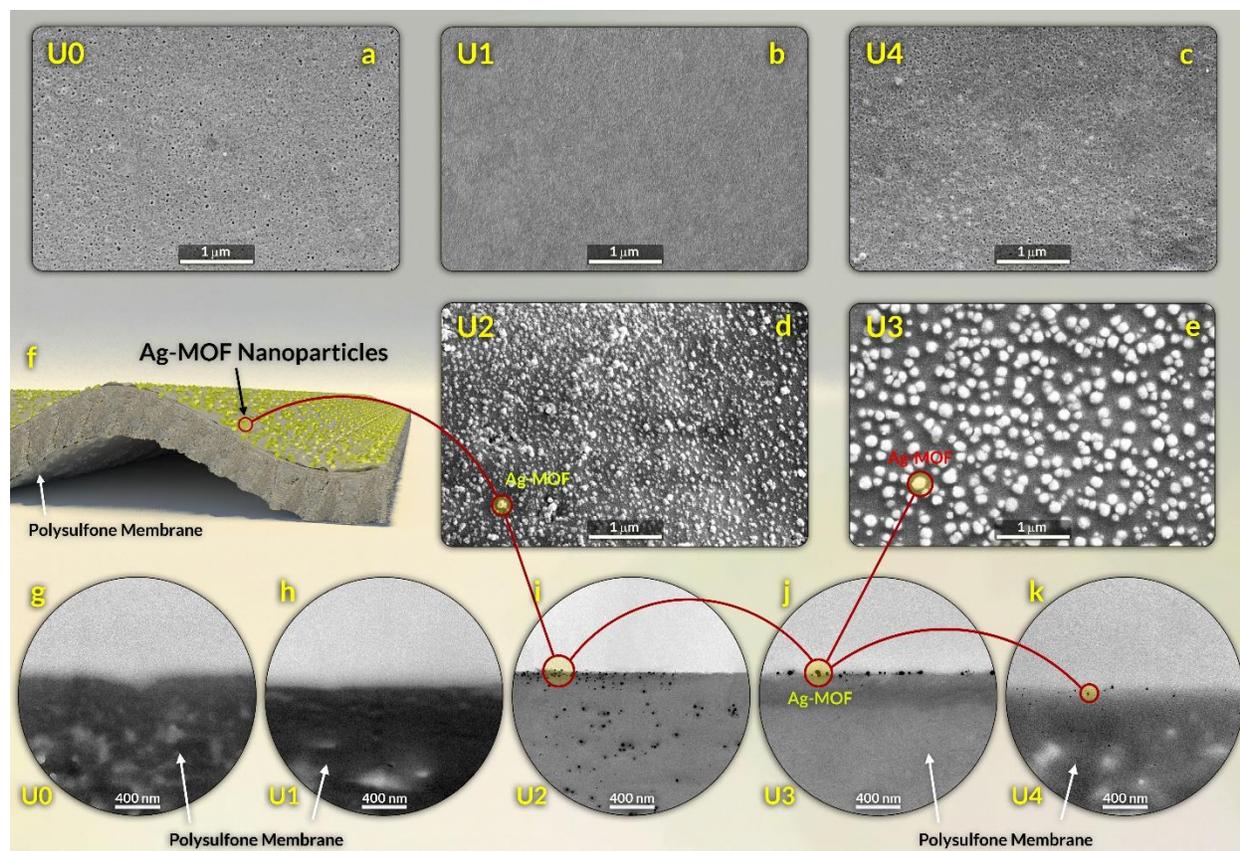
Figure 3. (a-e) SEM micrographs and (g-k) TEM micrographs of pristine and surface-modified membranes, and (f) schematic 3D illustration of the UF membranes modified with Ag-MOFs.

It is interesting to mention that the absence of photo-initiator-induced grafting of AA suppressed the deposition of Ag-MOFs, as observed for U4, on which bulky and irregular clusters are visible, resulting in a non-uniform and sparse distribution of nanomaterials (Figure 3k). This result is likely due to a relatively weaker binding to the surface manifesting itself in terms of easy remobilization and likely translating into quick leaching and lower membrane longevity during operation. A complementary analysis of the membrane elemental composition was gathered through EDX measurements (Table 1). These data further corroborate the presence

of silver on the surface of U2, U3, and U4 to varying degrees. They also support the observations discussed above regarding the amount of silver in the order U3 > U2 >> U4.

Table 1. EDX data indicating the chemical composition of membrane surfaces in atomic percentage

|	U0	U1	U2	U3	U4
C%	69.1	57.4	57.4	45.4	60.4
N%	-	5.2	4.4	7.6	5.1
O%	11.4	11.9	14.9	16.4	10.7
S%	19.5	25.5	20.8	14.9	23.8
Ag%	-	-	2.6	15.6	0.03

3.1.3 Contact angles and wettability

Evaluation of the surface wettability can indirectly indicate the presence of functional coatings on the membrane surface. More importantly, wettability directly impacts membrane performance, especially to mitigate the deposition rate of hydrophobic, organic, and biological foulants. The water contact angles of the pristine and modified surfaces (Figure 4a) showed reduction upon functionalization from U0 through U3, with the best value achieved for U3, i.e., for the membranes with in-situ grown MOFs on the top of BP-activated AA-coated samples. U2 and U3 (Ag-MOFs and AA) exhibited lower contact angles and thus more wettable surfaces compared to U1 (solely AA), suggesting that both the anionic polymer and the MOFs imparted hydrophilicity to the surfaces. This phenomenon has been attributed to the presence of ionic silver in MOFs [28, 29] and COOH groups in AA [55, 56]. The lower contact angle value of U3 than U2 is likely due to the higher Ag-MOFs density on the surface of U3 (see Table 1) [57, 58].

3.1.4 Roughness analysis

For further insight into the morphology, the AFM scans of these membranes are provided in Figure 4b-f. The surface roughness parameters of pristine and modified samples were also measured and presented in Figure 4. All four of the modified samples exhibited a heightened roughness following UV-curing of additives, relative to pristine U0, consistent with what was visually observed in SEM micrographs. Slightly higher roughness was also determined for U2 compared to U3, possibly due to some MOF aggregates deposited onto the surface, which did not occur for U3 given the different MOF modification pathway and despite the larger MOF size on this membrane. This result suggests that the uniformity of MOF distribution may be advantageous when these materials are grown in-situ, thus avoiding issues with aggregate formation and deposition from the suspension.

Comparative examination of all U2 and U3 characterization results showed that U3 gained superior combined characteristics in terms of water affinity, surface roughness, and Ag-MOFs formation and loading, favouring the immobilization of MOFs on an established hydrophilic receptive layer rather than competition for binding sites when in a AA suspension. U4 did not significantly outperform U0 in surface features and Ag content, emphasizing the impact of the AA layer presence. Overall, it can be inferred that a layered and in-situ modification scheme yielded the best physio-chemical and morphological properties.
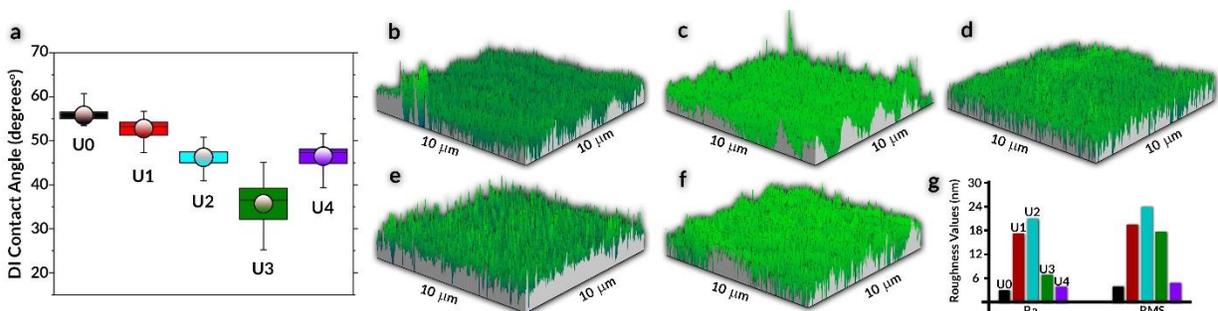
Figure 4. (a) Statistics of the contact angle of water droplets; 3D AFM images of (b) U0, (c) U1, (d) U2, (e) U3, and (f) U4 membranes; (g) AFM roughness parameters

3.2 Antibacterial Properties of the Membranes

The antibacterial activity of the membranes was tested by confocal microscopy using *E. coli* and *S. aureus* as gram-negative and gram-positive model bacteria, respectively (Figure 5a, b). U0 membrane showed nearly no antibacterial activity upon microbial contact with the surface from the suspensions (Figure $5a_0$, b_0). Instead, U2 and U3 provided 80% and 90% *E. coli* inactivation, respectively, and similar activity against *S. aureus* with 95% inactivation. U1 and U4 inhibited 10% and 17% of *E. coli*, and 3% and 13% of *S. aureus*, respectively. To further investigate the antibacterial activity of the membranes, disc inhibition zone tests were carried out, and the corresponding results are shown in Figure 5c, d. Only U2 and U3 showed inhibited areas around the membrane, consistent with the mortality rate of the bacteria cells observed in viability tests.

The results suggest that the main anti-bacterial properties stem from the activity of Ag-MOFs [59]. Ag-MOFs are a rich source of silver ions. The 3D structure of MOFs can be tailored to control and optimize the gradual release of silver ions, addressing undesired ion leaching from the membrane during the filtration process [60]. The reactive oxygen species of the organic linker may also play a part in the antibacterial activity [61], but those biocidal mechanisms are

unlikely to make a substantial contribution in these modified membranes. The accessibility of silver ions to the microbial cell is crucial to achieving bacterial inactivation. Combining confocal and inhibition zone results enable to better discuss the possible antibacterial mechanisms of membranes and provide insight into the relative importance of antibacterial agents that are strongly attached to the surface and those that are released. An inhibition zone forms around the membranes when antibacterial agents are released from the membranes and its results are mainly related to this antibacterial mechanism [62]. However, formation of an inhibition zone is not a guarantee for achieving a long-term antibacterial property [63, 64]. For long-lasting antifouling and antibiofouling activity, cells attached on the membrane surface should be inactivated [2] and this mechanism can be assessed with confocal microscopy, which thus mainly provides insight into the contribution of membrane functional materials that are bonded strongly to the surface [65, 66]. The stronger binding of MOFs grown in-situ on the surface of U3 samples instead of deposited and later reacted on U2, is consistent with the larger inactivation rate observed for the former samples (Figure 5 a2, b2 vs. a3, b3).
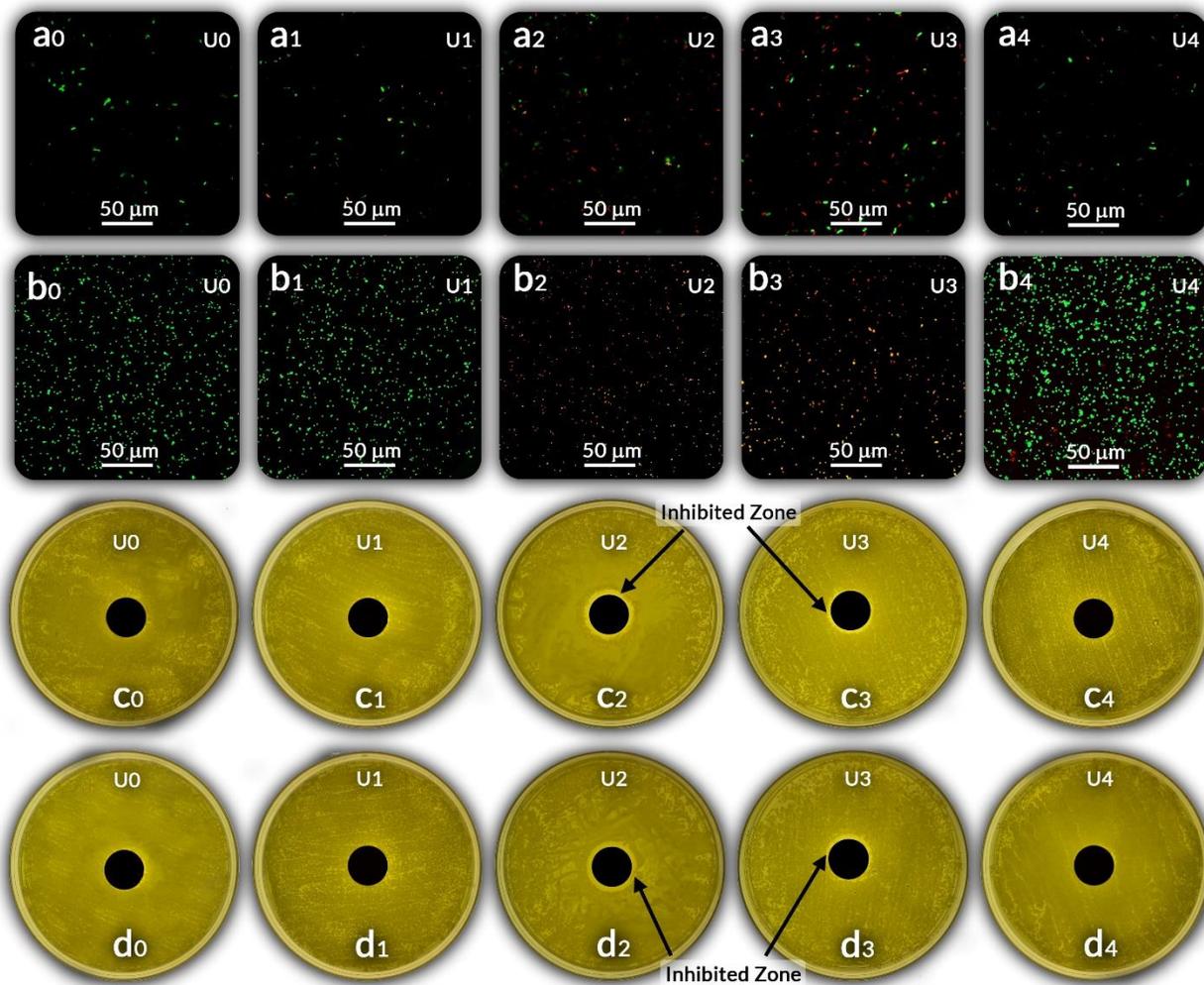
Figure 5. Assessment of the antibacterial activity of the membranes. Confocal images of the membranes upon surface contact with suspensions of (a) *E. coli*, and (b) *S. aureus*. Representative disc inhibition zones of the membranes with (c) *E. coli*, and (d) *S. aureus*. U0 (a0, b0, c0, and d0), U1 (a1, b1, c1, and d1), U2 (a2, b2, c2, and d2), U3 (a3, b3, c3, and d3), and U4 (a4, b4, c4, and d4).

3.3 Separation performance of the modified membranes

The PWP of pristine membranes was determined to be between 1500 and 2500 L m^{-1}h^{-1}bar^{-1}, with variability due to differences in surface porosity and pore size among different portions of the flat sheet commercial membrane. The modified membranes exhibited instead less PWP variations, which were also more consistent among the different sets of functionalization,

namely, 1200 ± 260 L m^{-1}h^{-1}bar^{-1}. These results are rationalized with the possibility that the additional AA and/or Ag-MOFs layers on U2, U3, and U4 membranes added some resistance to permeation and represented the main factor affecting mass transport, thus overriding the variability of the underlying membrane [67].

To evaluate organic fouling, the normalized flux of pristine and modified membranes was measured in long-term HA filtration tests, as shown in Figure 6a. Grafting AA and MOFs on top of the PSf surfaces improved the fouling resistance of the membrane, as these modifications: (i) lowered the rate of initial flux decline; and (ii) increased the value of steady flux at the end of the fouling run. The steady fluxes were roughly 7 (U1), 3 (U2). 13 (U3), and 5 (U4) times higher than the flux measured with the pristine membrane. This result is especially notable for U3, which had the largest wettability from contact angle tests. The initial flux decline rate was high for all samples. This result is consistent with the composition of the feed solution, comprising HA and divalent cations at high concentration to promote accelerated fouling conditions, as well as with the dead-end configuration of the experimental cell, promoting the quick formation of a cake layer upon rejection of HA by the membrane. However, the initial flux decline of U0 pristine samples was roughly 36%, 30%, 44%, and 19% faster compared to U1, U2, U3, and U4, respectively, further indicating the impact of surface functionalization on the fouling propensity of the membranes.
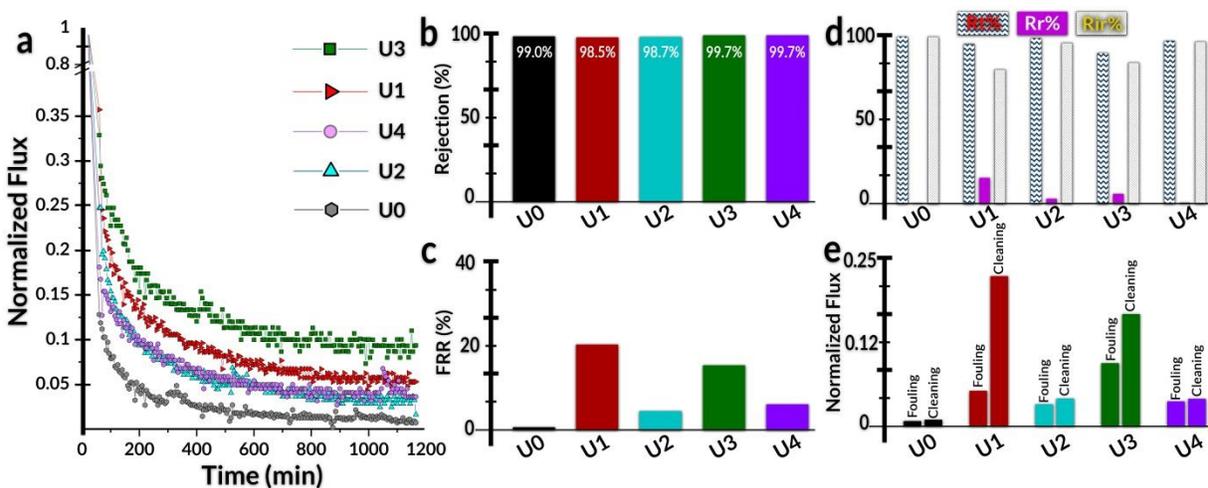
Figure 6. (a) Normalized flux of pristine and modified membranes in long term humic acids (HA) fouling filtration; (b) observed rejection of HA; (c) normalized flux recovery ratio (in percentage) subsequent to physical cleaning; (d) different components of membrane fouling, categorized into total fouling ($R_t\%$), irreversible fouling ($R_{ir}\%$), and reversible fouling ($R_r\%$); and (e) comparison between fluxes at the end of HA filtration ("fouling") and DI fluxes following membrane cleaning.

HA rejection was also measured for each membrane (Figure 6b). High rejection (>98.5%) was maintained in all samples after surface modification, with some samples exhibiting up to 99.7% rejection. The flux recovery ratio (FRR%) was calculated and plotted in Figure 6c to further understand the anti-fouling behavior of the membranes, specifically, the reversibility of foulant deposition and physical cleaning efficiency. U1 and U3 with FRR% of 20% and 16%, respectively, suggested a better cleaning behavior compared to other samples. Interestingly, looking into reversible and irreversible constituents of total fouling revealed that a higher relative percentage of total fouling was reversible for U1 (15%), followed by U3 (6%), as summarized in Figure 6d. Notably, the pristine membrane (U0) was characterized by near 100% irreversible fouling. While the fouling parameters improved significantly for U1 and U3 membranes compared to pristine samples, it should be underlined that the reversible fouling increased only

25

slightly. When surfaces become more wettable following modification, especially U3 in this study (Figure 4), the higher surface energy may lead to a lower likelihood of foulant adhesion to the membrane but not necessarily accompanied by an enhanced detachment probability once a foulant layer is formed, as also pointed out by previous studies [68, 69]. This phenomenon may partly explain the low fraction of reversible fouling estimated for the modified membranes despite their significantly lower flux decline, and it suggests that the membrane should be operated by avoiding extensive fouling layer formation and with relatively frequent physical cleaning, albeit less frequent than for pristine membranes.

In summary, U1 outperformed U0 by a wide margin in every performance metric, due to the existence of a hydrophilic AA layer. The use of Ag-MOFs was also favourable to antifouling activity and permeation performance of the U3 membranes. The higher surface roughness and lower wettability of U2 led to relatively more fouling susceptibility and irreversibility of this membrane [70-72]. Simply depositing MOFs on pristine membranes (U4) or surfaces previously coated with AA (U2) was not a suitable strategy for surface modification. Instead, U3, obtained by pre-hydrophilizing the material with AA and exploiting this coating to grow uniform Ag-MOFs provided the best overall combination of wettability, roughness, productivity, and rejection. U3 also had a strong biocidal activity, which would act as a barrier against microbial deposition and biofilm formation.

3.4 Release of silver ions

The robustness of silver-containing MOFs immobilized onto the polymeric membrane surfaces was assessed by measuring the rate of silver release, a paramount parameter to maintain a contact-based "defensive" bacterial inactivation and a dissolution approach for "offensive"

killing [4]. A 15-day silver release monitoring was conducted on U2, U3, and U4 samples (Figure 7). U3 and U4 showed a relatively low and steady release rate while U2 displayed an initially high value of silver release, which quickly dropped to values similar to those measured with U4 (Figure 7a). As discussed above, AA significantly boosted Ag-MOFs loading onto U2 and U3 samples by potentially providing hospitable binding sites through carboxyl groups, which would explain the larger rates of release for these two samples (Figure 7b). While in U3 samples all the MOFs are virtually linked to AA "roots", the procedure applied to deposit MOFs onto U2 membranes may result in several loosely bound nanoparticles that may have been detached from the surface during the first few days of monitoring. Overall, U3 showed an advantage in terms of MOF release rate, with no more than 0.2 ppm of silver measured in solution after 15 days. These results agree with the larger inhibition zone around U2 samples, for which a higher release rate was observed.

According to WHO guidelines, a silver concentration of up to 0.1 mg/L in drinking water could be deemed tolerable for humans if they were to consume said water source concentration for 70 years. In such a way, the human body would intake only half of the maximum no-observed-adverse-effect-level (NOAEL) of 10 g. The silver release for U3 and U4 amounted to a cumulative concentration of 0.2 mg/L during their 15-day batch release tests, corresponding to silver mass leaching rates around 0.03-0.04 mg $m^{-2}h^{-1}$. This figure would translate into a concentration range of roughly 0.1-1 μg/L in typical cross-flow hollow fibre ultrafiltration modules under real-scale flow conditions, thus at least two orders of magnitude lower than the WHO guidelines. The relatively low leaching values suggest that Ag-MOFs were securely bound to PSf membranes via UV-grafting for long-lasting biocidal activity in aqueous environments.

Moreover, it can be concluded that these membranes would not pose a significant safety hazard to human health.
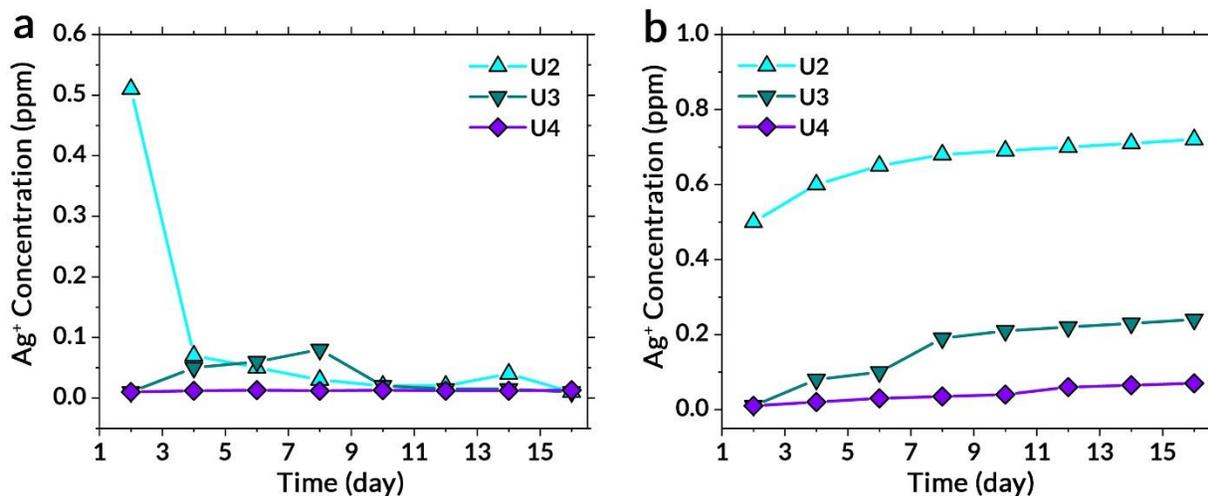
Figure 7. Silver ion leaching results for the membranes modified with Ag-MOFs. Test results were reported in a) daily amounts and b) cumulative amounts for the total duration of 15 days.

4. Conclusions

Biocidal Ag-MOFs immobilization was carried out through photo-initiator-assisted UV-grafting and their efficacy of the resulting ultrafiltration membranes was evaluated. Benzophenone was used as the photo-initiator and acrylic acid was applied to render the surface more hydrophilic and provide sites for further Ag-MOFs functionalization to achieve target antibacterial and antifouling properties. Different modification strategies were investigated: the pre-coating with acrylic acid proved necessary to obtain a high-density MOF modification of the surface. Specifically, the in-situ seeding and growth of these biocidal nanomaterials was the most effective approach to maximize the uniformity of surface functionalization and impart the desired new functions to the membrane while maintaining the advantageous inherent characteristics of the polymeric membrane. The samples were studied under ultrafiltration

conditions to assess their separation properties, including productivity, antifouling activity, and organic rejection. In all cases, the surface modification was achieved while maintaining or significantly improve said properties. The best membranes had up to 3 times the flux of pristine membranes, 15% fouling reversibility (compared to almost zero for the pristine membrane), and 20% cleaning efficiency (compared to < 0.1%). The MOF-containing membranes were tested for antibacterial activity against *E. coli* and *S. aureus* and reached up to 90% and 95% inactivation rates upon simple contact, respectively. The rate of silver release from the immobilized MOFs suggested adequate immobilization and long-term performance potential. Overall, the membrane referred to as U3, obtained with in-situ growth of MOFs on the acrylic acid UV-grafted support, proved to be the most effective in terms of combined: (i) controlled surface features, (ii) enhanced separation properties, (iii) lower fouling propensity, (iv) strong antibacterial activity, and (v) potentially prolonged antifouling potency coupled with biocidal propensity. This study proves that UV-grafting and application of metal-organic frameworks can be successfully achieved and provide the ground for further tailoring of ultrafiltration membranes with the goal of increased water production and water quality with lower overall energy consumption and increased ease of operation.

AUTHOR INFORMATION

Corresponding Authors

Alberto Tiraferri – *Politecnico di Torino, Turin, Italy*; Email: alberto.tiraferri@polito.it

Ahmad Rahimpour – *Babol Noshirvani University of Technology, Babol, Iran*; Email: ahmadrahimpour@nit.ac.ir

Mark Elliott – *The University of Alabama, Tuscaloosa, AL, USA* – Email: melliott@eng.ea.edu

Declaration of Competing Interest

Acknowledgments

References

[1]   X. Zhu, D. Jassby, Electroactive Membranes for Water Treatment: Enhanced Treatment Functionalities, Energy Considerations, and Future Challenges, Acc. Chem. Res. 52 (2019) 1177-1186. https://doi.org/10.1021/acs.accounts.8b00558.

[2]   M.D. Firouzjaei, S.F. Seyedpour, S.A. Aktij, M. Giagnorio, N. Bazrafshan, A. Mollahosseini, F. Samadi, S. Ahmadalipour, F.D. Firouzjaei, M.R. Esfahani, A. Tiraferri, M. Elliott, M. Sangermano, A. Abdelrasoul, J.R. McCutcheon, M. Sadrzadeh, A.R. Esfahani, A. Rahimpour, Recent advances in functionalized polymer membranes for biofouling control and mitigation in forward osmosis, J. Membr. Sci. 596 (2020) 117604. https://doi.org/10.1016/j.memsci.2019.117604.

[3]   Y. Chen, W. Xu, H. Zhu, D. Wei, F. He, D. Wang, B. Du, Q. Wei, Effect of turbidity on micropollutant removal and membrane fouling by MIEX/ultrafiltration hybrid process, Chemosphere 216 (2019) 488-498. https://doi.org/10.1016/j.chemosphere.2018.10.148.

[4]   M.S. Mauter, Y. Wang, K.C. Okemgbo, C.O. Osuji, E.P. Giannelis, M. Elimelech, Antifouling ultrafiltration membranes via post-fabrication grafting of biocidal nanomaterials, ACS Appl. Mater. Interfaces 3 (2011) 2861-2868. https://doi.org/10.1021/am200522v.

[5]   X. Shi, G. Tal, N.P. Hankins, V. Gitis, Fouling and cleaning of ultrafiltration membranes: A review, J. Water Process. Eng. 1 (2014) 121-138. https://doi.org/10.1016/j.jwpe.2014.04.003.

[6]   W. Yuan, A.L. Zydney, Humic Acid Fouling during Ultrafiltration, Environ. Sci. Technol. 34 (2000) 5043-5050. https://doi.org/10.1021/es0012366.

[7]   K. Kimura, Y. Hane, Y. Watanabe, G. Amy, N. Ohkuma, Irreversible membrane fouling during ultrafiltration of surface water, Water Res. 38 (2004) 3431-3441. https://doi.org/10.1016/j.watres.2004.05.007.

[8]   M.R. Esfahani, S.A. Aktij, Z. Dabaghian, M.D. Firouzjaei, A. Rahimpour, J. Eke, I.C. Escobar, M. Abolhassani, L.F. Greenlee, A.R. Esfahani, A. Sadmani, N. Koutahzadeh, Nanocomposite membranes for water separation and purification: Fabrication, modification, and applications, Sep. Purif. Technol. 213 (2019) 465-499. https://doi.org/10.1016/j.seppur.2018.12.050.

[9]   K. Scott, R. Hughes, Industrial Membrane Separation Technology, ed., Springer Netherlands, 1996.

[10]   A. Zirehpour, A. Rahimpour, A. Arabi Shamsabadi, M. Sharifian Gh, M. Soroush, Mitigation of Thin-Film Composite Membrane Biofouling via Immobilizing Nano-Sized Biocidal Reservoirs in the Membrane Active Layer, Environ. Sci. Technol. 51 (2017) 5511-5522. https://doi.org/10.1021/acs.est.7b00782.

[11]   S.B. Darling, Perspective: Interfacial materials at the interface of energy and water, J. Appl. Phys. 124 (2018) 30901-30901. https://doi.org/10.1063/1.5040110.

[12]   M. Ganj, M. Asadollahi, S.A. Mousavi, D. Bastani, F. Aghaeifard, Surface modification of polysulfone ultrafiltration membranes by free radical graft polymerization of acrylic acid using response surface methodology, J. Polym. Res. 26 (2019) 1-19. https://doi.org/10.1007/s10965-019-1832-3.

[13]   H. Basri, A.F. Ismail, M. Aziz, Polyethersulfone (PES)–silver composite UF membrane: Effect of silver loading and PVP molecular weight on membrane morphology and antibacterial activity, Desalination 273 (2011) 72-80. https://doi.org/10.1016/j.desal.2010.11.010.

[14]   M. Rai, A. Yadav, A. Gade, Silver nanoparticles as a new generation of antimicrobials, Biotechnol. Adv. 27 (2009) 76-83. https://doi.org/10.1016/j.biotechadv.2008.09.002.

[15]   S.F. Seyedpour, A. Rahimpour, G. Najafpour, Facile in-situ assembly of silver-based MOFs to surface functionalization of TFC membrane: A novel approach toward long-lasting biofouling mitigation, J. Membr. Sci. 573 (2019) 257-269. https://doi.org/10.1016/j.memsci.2018.12.016.

[16]   M. Ben-Sasson, K.R. Zodrow, Q. Genggeng, Y. Kang, E.P. Giannelis, M. Elimelech, Surface functionalization of thin-film composite membranes with copper nanoparticles for antimicrobial surface properties, Environ. Sci. Technol. 48 (2014) 384-393. https://doi.org/10.1021/es404232s.

[17]   D.J. Miller, P.A. Araújo, P.B. Correia, M.M. Ramsey, J.C. Kruithof, M.C.M. van Loosdrecht, B.D. Freeman, D.R. Paul, M. Whiteley, J.S. Vrouwenvelder, Short-term adhesion and long-term biofouling testing of polydopamine and poly(ethylene glycol) surface modifications of membranes and feed spacers for biofouling control, Water Res. 46 (2012) 3737-3753. https://doi.org/10.1016/j.watres.2012.03.058.

[18]   M. He, X. Fan, Z. Yang, R. Zhang, Y. Liu, L. Fan, Q. Zhang, Y. Su, Z. Jiang, Antifouling high-flux membranes via surface segregation and phase separation controlled by the synergy of hydrophobic and hydrogen bond interactions, J. Membr. Sci. 520 (2016) 814-822. https://doi.org/10.1016/j.memsci.2016.08.044.

[19]   S. Kitagawa, R. Kitaura, S.I. Noro, Functional porous coordination polymers, Angew. Chem. Int. 43 (2004) 2334-2375. https://doi.org/10.1002/anie.200300610.

[20]   N. Yin, K. Wang, L. Wang, Z. Li, Amino-functionalized MOFs combining ceramic membrane ultrafiltration for Pb (II) removal, Chem. Eng. J. 306 (2016) 619-628. https://doi.org/10.1016/j.cej.2016.07.064.

[21]   M.D. Firouzjaei, A.A. Shamsabadi, M. Sharifian Gh, A. Rahimpour, M. Soroush, A Novel Nanocomposite with Superior Antibacterial Activity: A Silver-Based Metal Organic Framework Embellished with Graphene Oxide, Adv. Mater. Interfaces 5 (2018) 1701365-1701365. https://doi.org/10.1002/admi.201701365.

[22]   M. Mozafari, S.F. Seyedpour, S.K. Salestan, A. Rahimpour, A.A. Shamsabadi, M.D. Firouzjaei, M.R. Esfahani, A. Tiraferri, H. Mohsenian, M. Sangermano, M. Soroush, Facile Cu-BTC surface modification of thin chitosan film coated polyethersulfone membranes with improved antifouling properties for sustainable removal of manganese, J. Membr. Sci. 588 (2019) 117200-117200. https://doi.org/10.1016/j.memsci.2019.117200.

[23]   G. Wyszogrodzka, B. Marszałek, B. Gil, P. Dorozyński, Metal-organic frameworks: Mechanisms of antibacterial action and potential applications, Drug. Discov. Today 21 (2016) 1009-1018. https://doi.org/10.1016/j.drudis.2016.04.009.

[24]   W. Ding, J. Cai, Z. Yu, Q. Wang, Z. Xu, Z. Wang, C. Gao, Fabrication of an aquaporin-based forward osmosis membrane through covalent bonding of a lipid bilayer to a microporous support, J. Mater. Chem. A 3 (2015) 20118-20126. https://doi.org/10.1039/c5ta05751e.

[25]   H.M. Hegab, A. ElMekawy, T.G. Barclay, A. Michelmore, L. Zou, C.P. Saint, M. Ginic-Markovic, Fine-Tuning the Surface of Forward Osmosis Membranes via Grafting Graphene Oxide: Performance Patterns and Biofouling Propensity, ACS Appl. Mater. Interfaces 7 (2015) 18004-18016. https://doi.org/10.1021/acsami.5b04818.

[26]   Q. Chen, P. Yu, W. Huang, S. Yu, M. Liu, C. Gao, High-flux composite hollow fiber nanofiltration membranes fabricated through layer-by-layer deposition of oppositely charged crosslinked polyelectrolytes for dye removal, J. Membr. Sci. 492 (2015) 312-321. https://doi.org/10.1016/j.memsci.2015.05.068.

[27]   Y.H. La, J. Diep, R. Al-Rasheed, D. Miller, L. Krupp, G.M. Geise, A. Vora, B. Davis, M. Nassar, B.D. Freeman, M. McNeil, G. Dubois, Enhanced desalination performance of polyamide bi-layer membranes prepared by sequential interfacial polymerization, J. Membr. Sci. 437 (2013) 33-39. https://doi.org/10.1016/j.memsci.2013.02.044.

[28]   M. Pejman, M. Dadashi Firouzjaei, S. Aghapour Aktij, P. Das, E. Zolghadr, H. Jafarian, A. Arabi Shamsabadi, M. Elliott, M. Sadrzadeh, M. Sangermano, A. Rahimpour, A. Tiraferri, In Situ Ag-MOF Growth on Pre-Grafted Zwitterions Imparts Outstanding Antifouling Properties to Forward Osmosis Membranes, ACS Appl. Mater. Interfaces 12 (2020) 36287-36300. https://doi.org/10.1021/acsami.0c12141.

[29]   M. Pejman, M.D. Firouzjaei, S.A. Aktij, P. Das, E. Zolghadr, H. Jafarian, A.A. Shamsabadi, M. Elliott, M.R. Esfahani, M. Sangermano, M. Sadrzadeh, E.K. Wujcik, A. Rahimpour, A. Tiraferri, Improved antifouling and antibacterial properties of forward osmosis membranes through surface modification with zwitterions and silver-based metal organic frameworks, J. Membr. Sci. 611 (2020). https://doi.org/10.1016/j.memsci.2020.118352.

[30]   S. Minko, Grafting on solid surfaces: "Grafting" to and "grafting from" methods, in: M. Stamm (Ed.) Polymer Surfaces and Interfaces, Springer Berlin Heidelberg, 2008, pp. 215-234.

[31]   I. Roppolo, A. Chiappone, K. Bejtka, E. Celasco, A. Chiodoni, F. Giorgis, M. Sangermano, S. Porro, A powerful tool for graphene functionalization : Benzophenone mediated UV-grafting, Carbon 77 (2014) 226-235. https://doi.org/10.1016/j.carbon.2014.05.025.

[32]   H. Ma, R.H. Davis, C.N. Bowman, Novel sequential photoinduced living graft polymerization, Macromolecules 33 (2000) 331-335. https://doi.org/10.1021/ma990821s.

[33]   S.L. Wu, F. Liu, H.C. Yang, S.B. Darling, Recent progress in molecular engineering to tailor organic-inorganic interfaces in composite membranes, Mol. Syst. Des. Eng. 5 (2020) 433-444. https://doi.org/10.1039/c9me00154a.

[34]   M.B.M.Y. Ang, S.H. Huang, M.W. Chang, C.L. Lai, H.A. Tsai, W.S. Hung, C.C. Hu, K.R. Lee, Ultraviolet-initiated graft polymerization of acrylic acid onto thin-film polyamide surface for improved ethanol dehydration performance of pervaporation membranes, Sep. Purif. Technol. 235 (2020) 116155-116155. https://doi.org/10.1016/j.seppur.2019.116155.

[35]   V. Vatanpour, M. Esmaeili, M. Safarpour, A. Ghadimi, J. Adabi, Synergistic effect of carboxylated-MWCNTs on the performance of acrylic acid UV-grafted polyamide nanofiltration membranes, React. Funct. Polym. 134 (2019) 74-84. https://doi.org/10.1016/j.reactfunctpolym.2018.11.010.

[36]   Y. Yi, H. Tu, X. Zhou, R. Liu, Y. Wu, D. Li, Q. Wang, X. Shi, H. Deng, Acrylic acid-grafted pre-plasma nanofibers for efficient removal of oil pollution from aquatic environment, J. Hazard. Mater. 371 (2019) 165-174. https://doi.org/10.1016/j.jhazmat.2019.02.085.

[37]   M. Hajibabaei, R. Zendehdel, Z. Panjali, Imidazole-Functionalized Ag/MOFs as Promising Scaffolds for Proper Antibacterial Activity and Toxicity Reduction of Ag Nanoparticles, J. Inorg. Organomet. Polym. Mater. 30 (2020) 4622-4626. https://doi.org/10.1007/s10904-020-01612-8.

[38]   X. Cao, M. Tang, F. Liu, Y. Nie, C. Zhao, Immobilization of silver nanoparticles onto sulfonated polyethersulfone membranes as antibacterial materials, Colloids Surf. B 81 (2010) 555-562. https://doi.org/10.1016/j.colsurfb.2010.07.057.

[39]   Y. Zhao, Y. Zhou, X. Wu, L. Wang, L. Xu, S. Wei, A facile method for electrospinning of Ag nanoparticles/poly (vinyl alcohol)/carboxymethyl-chitosan nanofibers, Appl. Surf. Sci. 258 (2012) 8867-8873. https://doi.org/10.1016/j.apsusc.2012.05.106.

[40]   N.A.A. Sani, W.J. Lau, A.F. Ismail, Morphologies and separation characteristics of polyphenylsulfone-based solvent resistant nanofiltration membranes: Effect of polymer concentration in casting solution and membrane pretreatment condition, Korean J. Chem. Eng. 32 (2015) 743-752. https://doi.org/10.1007/s11814-014-0281-2.

[41]   Z. Yang, Y. Dai, S. Wang, H. Cheng, J. Yu, In situ incorporation of a S, N doped carbon/sulfur composite for lithium sulfur batteries, RSC Adv. 5 (2015) 78017-78025. https://doi.org/10.1039/c5ra15360c.

[42]   W. Xie, A. Tiraferri, X. Ji, C. Chen, Y. Bai, J.C. Crittenden, B. Liu, Green and sustainable method of manufacturing anti-fouling zwitterionic polymers-modified poly(vinyl chloride) ultrafiltration membranes, J. Colloid Interface Sci. 591 (2021) 343-351. https://doi.org/10.1016/j.jcis.2021.01.107.

[43]   S.F. Seyedpour, M. Dadashi Firouzjaei, A. Rahimpour, E. Zolghadr, A. Arabi Shamsabadi, P. Das, F. Akbari Afkhami, M. Sadrzadeh, A. Tiraferri, M. Elliott, Toward Sustainable Tackling of Biofouling Implications and Improved Performance of TFC FO Membranes Modified by Ag-MOF Nanorods, ACS Appl. Mater. Interfaces 12 (2020) 38285-38298. https://doi.org/10.1021/acsami.0c13029.

[44]   K. Singh, S. Devi, H.C. Bajaj, P. Ingole, J. Choudhari, H. Bhrambhatt, Optical Resolution of Racemic Mixtures of Amino Acids through Nanofiltration Membrane Process, Sep. Sci. Technol. 49 (2014) 2630-2641. https://doi.org/10.1080/01496395.2014.911023.

[45]   S. Rafiq, Z. Man, S. Maitra, A. Maulud, F. Ahmad, N. Muhammad, Preparation of asymmetric polysulfone/polyimide blended membranes for CO2 separation, Korean J. Chem. Eng. 28 (2011) 2050-2056. https://doi.org/10.1007/s11814-011-0053-1.

[46]   X. Wei, Z. Wang, J. Wang, S. Wang, A novel method of surface modification to polysulfone ultrafiltration membrane by preadsorption of citric acid or sodium bisulfite, Membr. Water Treat. 3 (2012) 35-49. https://doi.org/10.12989/mwt.2012.3.1.035.

[47]   C.Y. Tang, Y.-N. Kwon, J.O. Leckie, Effect of membrane chemistry and coating layer on physiochemical properties of thin film composite polyamide RO and NF membranes: I. FTIR and XPS characterization of polyamide and coating layer chemistry, Desalination 242 (2009) 149-167. https://doi.org/10.1016/j.desal.2008.04.003.

[48]   G. Xue, Q. Dai, S. Jiang, Chemical reactions of imidazole with metallic silver studied by the use of SERS and XPS techniques, J. Am. Chem. Soc. 110 (1988) 2393-2395. https://doi.org/10.1021/ja00216a009.

[49]   J. Yang, H. Bai, X. Tan, J. Lian, IR and XPS investigation of visible-light photocatalysis—Nitrogen–carbon-doped TiO2 film, Appl. Surf. Sci. 253 (2006) 1988-1994. https://doi.org/10.1016/j.apsusc.2006.03.078.

[50]   I. Kusunoki, M. Sakai, Y. Igari, S. Ishidzuka, T. Takami, T. Takaoka, M. Nishitani-Gamo, T. Ando, XPS study of nitridation of diamond and graphite with a nitrogen ion beam, Surf. Sci. 492 (2001) 315-328. https://doi.org/10.1016/S0039-6028(01)01430-3.

[51]   B.J. Matsoso, K. Ranganathan, B.K. Mutuma, T. Lerotholi, G. Jones, N.J. Coville, Synthesis and characterization of boron carbon oxynitride films with tunable composition using methane, boric acid and ammonia, New J. Chem. 41 (2017) 9497-9504. https://doi.org/10.1039/C7NJ01886J.

[52]   J. Ye, F. He, J. Nie, Y. Cao, H. Yang, X. Ai, Sulfur/carbon nanocomposite-filled polyacrylonitrile nanofibers as a long life and high capacity cathode for lithium–sulfur batteries, J. Mater. Chem. A 3 (2015) 7406-7412. https://doi.org/10.1039/C4TA06976E.

[53]   A. Abdul Razzaq, Y. Yao, R. Shah, P. Qi, L. Miao, M. Chen, X. Zhao, Y. Peng, Z. Deng, High-performance lithium sulfur batteries enabled by a synergy between sulfur and carbon nanotubes, Energy Storage Mater. 16 (2019) 194-202. https://doi.org/10.1016/j.ensm.2018.05.006.

[54]   R. Liu, Z. Xian, S. Zhang, C. Chen, Z. Yang, H. Li, W. Zheng, G. Zhang, H. Cao, Electrochemical-reduction-assisted assembly of ternary Ag nanoparticles/polyoxometalate/graphene nanohybrids and their activity in the electrocatalysis of oxygen reduction, RSC Adv. 5 (2015) 74447-74456. https://doi.org/10.1039/C5RA12556A.

[55]   B. Deng, M. Yu, X. Yang, B. Zhang, L. Li, L. Xie, J. Li, X. Lu, Antifouling microfiltration membranes prepared from acrylic acid or methacrylic acid grafted poly(vinylidene fluoride) powder synthesized via pre-irradiation induced graft polymerization, J. Membr. Sci. 350 (2010) 252-258. https://doi.org/10.1016/j.memsci.2009.12.035.

[56]   L. Shen, Y. Zhang, W. Yu, R. Li, M. Wang, Q. Gao, J. Li, H. Lin, Fabrication of hydrophilic and antibacterial poly(vinylidene fluoride) based separation membranes by a novel strategy combining radiation grafting of poly(acrylic acid) (PAA) and electroless nickel plating, J. Colloid Interface Sci. 543 (2019) 64-75. https://doi.org/10.1016/j.jcis.2019.02.013.

[57]   M.F. Ismail, B. Khorshidi, M. Sadrzadeh, New insights into the impact of nanoscale surface heterogeneity on the wettability of polymeric membranes, J. Membr. Sci. 590 (2019) 117270. https://doi.org/10.1016/j.memsci.2019.117270.

[58]   K. Seo, M. Kim, D.H. Kim, Re-derivation of Young's Equation, Wenzel Equation, and Cassie-Baxter Equation Based on Energy Minimization, in: M. Aliofkhazraei (Ed.) Surface Energy, Intech Open, 2015, pp.

[59]   S.F. Seyedpour, A. Arabi Shamsabadi, S. Khoshhal Salestan, M. Dadashi Firouzjaei, M. Sharifian Gh, A. Rahimpour, F. Akbari Afkhami, M.R. Shirzad Kebria, M.A. Elliott, A. Tiraferri, M. Sangermano, M.R. Esfahani, M. Soroush, Tailoring the Biocidal Activity of Novel

Silver-Based Metal Azolate Frameworks, ACS Sustainable Chem. Eng. 8 (2020) 7588-7599. https://doi.org/10.1021/acssuschemeng.0c00201.

[60] M. Dadashi Firouzjaei, F. Akbari Afkhami, M. Rabbani Esfahani, C.H. Turner, S. Nejati, Experimental and molecular dynamics study on dye removal from water by a graphene oxide-copper-metal organic framework nanocomposite, J. Water Process. Eng. 34 (2020) 101180-101180. https://doi.org/10.1016/j.jwpe.2020.101180.

[61] J. Zhu, J. Hou, Y. Zhang, M. Tian, T. He, J. Liu, V. Chen, Polymeric antimicrobial membranes enabled by nanomaterials for water treatment, J. Membr. Sci. 550 (2018) 173-197. https://doi.org/10.1016/j.memsci.2017.12.071.

[62] J. Lin, X. Chen, C. Chen, J. Hu, C. Zhou, X. Cai, W. Wang, C. Zheng, P. Zhang, J. Cheng, Z. Guo, H. Liu, Durably Antibacterial and Bacterially Antiadhesive Cotton Fabrics Coated by Cationic Fluorinated Polymers, ACS Appl. Mater. Interfaces 10 (2018) 6124-6136. https://doi.org/10.1021/acsami.7b16235.

[63] X. Liu, S. Qi, Y. Li, L. Yang, B. Cao, C.Y. Tang, Synthesis and characterization of novel antibacterial silver nanocomposite nanofiltration and forward osmosis membranes based on layer-by-layer assembly, Water Res. 47 (2013) 3081-3092. https://doi.org/10.1016/j.watres.2013.03.018.

[64] K. Zodrow, L. Brunet, S. Mahendra, D. Li, A. Zhang, Q. Li, P.J.J. Alvarez, Polysulfone ultrafiltration membranes impregnated with silver nanoparticles show improved biofouling resistance and virus removal, Water Res. 43 (2009) 715-723. https://doi.org/10.1016/j.watres.2008.11.014.

[65] H.C. Pappas, S. Phan, S. Yoon, L.E. Edens, X. Meng, K.S. Schanze, D.G. Whitten, D.J. Keller, Self-Sterilizing, Self-Cleaning Mixed Polymeric Multifunctional Antimicrobial Surfaces, ACS Appl. Mater. Interfaces 7 (2015) 27632-27638. https://doi.org/10.1021/acsami.5b06852.

[66] A. Rahimpour, S.F. Seyedpour, S. Aghapour Aktij, M. Dadashi Firouzjaei, A. Zirehpour, A. Arabi Shamsabadi, S. Khoshhal Salestan, M. Jabbari, M. Soroush, Simultaneous Improvement of Antimicrobial, Antifouling, and Transport Properties of Forward Osmosis Membranes with Immobilized Highly-Compatible Polyrhodanine Nanoparticles, Environ. Sci. Technol. 52 (2018) 5246-5258. https://doi.org/10.1021/acs.est.8b00804.

[67] D. Ma, S.B. Peh, G. Han, S.B. Chen, Thin-Film Nanocomposite (TFN) Membranes Incorporated with Super-Hydrophilic Metal–Organic Framework (MOF) UiO-66: Toward Enhancement of Water Flux and Salt Rejection, ACS Appl. Mater. Interfaces 9 (2017) 7523-7534. https://doi.org/10.1021/acsami.6b14223.

[68] A. Tiraferri, Y. Kang, E.P. Giannelis, M. Elimelech, Superhydrophilic Thin-Film Composite Forward Osmosis Membranes for Organic Fouling Control: Fouling Behavior and Antifouling Mechanisms, Environ. Sci. Technol. 46 (2012) 11135-11144. https://doi.org/10.1021/es3028617.

[69] A. Tiraferri, Y. Kang, E.P. Giannelis, M. Elimelech, Highly Hydrophilic Thin-Film Composite Forward Osmosis Membranes Functionalized with Surface-Tailored Nanoparticles, ACS Appl. Mater. Interfaces 4 (2012) 5044-5053. https://doi.org/10.1021/am301532g.

[70] F. Gholami, S. Zinadini, A.A. Zinatizadeh, A.R. Abbasi, TMU-5 metal-organic frameworks (MOFs) as a novel nanofiller for flux increment and fouling mitigation in PES

ultrafiltration membrane, Sep. Purif. Technol. 194 (2018) 272-280. https://doi.org/10.1016/j.seppur.2017.11.054.

[71]   F. Mohammadnezhad, M. Feyzi, S. Zinadini, A novel Ce-MOF/PES mixed matrix membrane; synthesis, characterization and antifouling evaluation, J. Ind. Eng. Chem. 71 (2019) 99-111. https://doi.org/10.1016/j.jiec.2018.09.032.

[72]   S. Yang, Q. Zou, T. Wang, L. Zhang, Effects of GO and MOF@GO on the permeation and antifouling properties of cellulose acetate ultrafiltration membrane, J. Membr. Sci. 569 (2019) 48-59. https://doi.org/10.1016/j.memsci.2018.09.068.